SAND2013-6198C

Optimal Resistive Control Strategy for a Floating OWC Device

Diana Bull[1], Erick Johnson[2]

[1]*Sandia National Laboratories*
Albuquerque, NM, USA
dlbull@sandia.gov

[2]*Montana State University*
Bozeman, MT, USA
erick.johnson@me.montana.edu

***Abstract*— A resistive control strategy to optimize pneumatic power for a floating OWC device is presented. This strategy utilizes a linear, frequency-domain performance model that links an oscillating structure to air-pressure fluctuations with a Wells Turbine in 3-dimensions. An array of field points defining the interior free surface allows hydrodynamic parameters relating to the fluctuating air-pressure within the OWC to be calculated using reciprocity relations. Device structural parameters for a non-optimized BBDB are detailed and the performance model is exercised on this device. A new resonance results from coupling the floating structure to the air-column that is unique from the uncoupled resonance location. An analytic expression for the optimal resistive load to link the floating structure and air-column dynamics is presented. When the optimal resistive load is exercised within the model, the natural resonances of the coupled system are preserved and additional linked peaks are identified. This formulation of the optimal resistive load is shown to contribute significantly to the device capture width and power performance.**

***Keywords*—wave energy, OWC, moonpool, BBDB, 3-dimensional frequency domain performance model, resistive damping control, Wells Turbine**

I. Introduction

An oscillating water column (OWC) is a class of wave energy converter (WEC). Essentially this WEC contains a moonpool, an opening in a partially submerged structure, with an air-chamber covering the free surface. The air-chamber is only open to the atmosphere through a turbine. The incident waves result in a fluctuating pressure within the air-chamber. Bidirectional air flow, caused by the difference in pressure within the air-chamber relative to the ambient outside, drives the turbine and produces an electrical power output. Often a self-rectifying turbine, like the Wells Turbine, is employed so that the turbine rotates only in one direction.

OWCs can be located offshore (OE Buoy [1], blueWAVE [2], Sperboy [3]), nearshore (greenWAVE [2]), or onshore (Pico [4], Limpet [5], Mutriku [6]). The deployment location strongly affects the requirements on the performance model. An offshore OWC will have to float, which uniquely requires that both the wave activated body and the OWC are modeled in a coupled fashion as each absorbs power from the waves. It is the relative motion between the device and the internal free surface that produces air flow in this case. Nearshore and onshore OWCs only require the pressure fluctuation from the internal free surface to be modeled, thus reducing the number of independent variables to be considered.

The radiated wave pattern (*i.e.* the wave pattern resulting from an oscillating device in still water) strongly influences the maximum theoretical power absorption by the device, see [7, Sec 6.1] for further discussion. This wave pattern is dependent upon both the modes of oscillation as well as the symmetry of the device. Thus a non-axisymmetric device oscillating in all six rigid body modes is expected to absorb power distinctly from an axisymmetric device similarly oscillating in all six rigid body modes.

In this paper an offshore (floating) OWC terminator is studied. The Backward Bent Duct Buoy (BBDB) design was first proposed by Masuda [8] in the 1980's and is one variety of floating OWC devices. This design is an L-shape with the opening to the ocean downstream from the wave propagation direction. The BBDB benefits from the coupled surge, heave, and pitch rigid-body modes and the OWC's resonance to expand the frequency range of efficient conversion. The natural resonance of the OWC is dependent upon both the length and free surface area of the water column [9] [10].

There are two approaches to modeling the free surface: a rigid weightless piston [11] or calculation of the pressure distribution [12] [13]. The first approach is only valid for small internal free surface areas and is akin to a 2-body treatment in which the oscillating structure and the OWC are treated independently. The second approach does not place limitations on the size of the internal free surface area and utilizes a Boundary Element Method (BEM) solver to model the dynamics of the floating body and the fluctuating air-pressure. Calculation of the internal pressure distribution, when using a BEM solver, can be obtained in three ways: approximated, solved for explicitly, or solved for implicitly [14] [15]. Approximation utilizes the technique of generalized modes [14] which expands upon the rigid piston approximation to include additional higher order modes. Explicit calculation requires determination of the velocity potential for the free surface. This is currently possible in WAMIT v7.0 [16], however this capability is new and uncommon in other potential flow solvers. Implicit calculation utilizes reciprocity relations to solve for all of the free surface parameters from the oscillating structure potential using an

array of field points on the internal free surface. Implicit calculation, presented in [15] and [7] and applied by [17], is pursued in this paper allowing for the use of standard potential flow solvers, such as WAMIT v6.4 [18].

This paper will present the impact on pneumatic power through the inclusion of body oscillations in the optimization of the OWC turbine control. In order to demonstrate this, a general BBDB design is described in Section II so as to discuss the 3-dimensional hydrodynamic model with results presented in Sections III and IV respectively. Section V develops the performance model, linked through a Wells Turbine, and presents an analytical solution to optimize resistive control. Finally, Section VI presents the results of optimizing resistive control of the Wells Turbine considering power absorbed by both the oscillating structure and fluctuating air-pressure.

II. Floating OWC Geometry

The BBDB is modeled to determine both the structural parameters, using SolidWorks [19], as well as the hydrodynamic parameters, using MultiSurf [20]. Fig. 1 illustrates the structural design, while Fig. 2 shows the hydrodynamic counterpart (note only the wetted surface must be modeled for the potential flow BEM solver). The majority of the device dimensions were selected based upon the conclusions of the following papers [21], [22], and [23]. This design profile is not optimized to reduce viscous losses or encourage weathervaning as is depicted in [1] and [17].

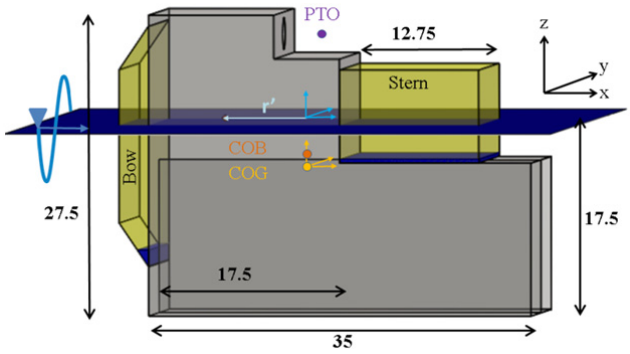

Fig. 1. Model of the OWC describing dimensions, locations of principal components, locations of the COB and COG, and identifying coordinate systems

The structural design assumes a uniform thickness of A36 steel, appropriate ballast mass and placement, and an estimate of the mass and location of the power conversion chain. An average wall thickness of 35.1 mm is applied to the entire device [24]. This average thickness was derived from a structural design engineered to withstand the hydrostatic pressure at a submergence of 25 m [25]. The ballast is distributed to obtain the desired draft and ensure that the center of gravity and the center of buoyancy are aligned vertically. The ballast is assumed to be seawater and is added to the buoyancy chambers as shown in Fig. 1. The mass of the power conversion chain (drivetrain, generator, power conditioning electronics) is approximated [26] and is placed at the expected center of the Wells Turbine location, also shown in Fig. 1. TABLE I summarizes the structural properties of the device that are needed as input into WAMIT.

Displaced Mass [kg]		2,024,657		
Structural Mass [kg]		1,808,944		
Bow Ballast Mass [kg]		22,072		
Stern Ballast Mass [kg]		123,641		
Power Conversion Mass [kg]		70,000		
COG (x,y,z) [m]		0.00	0.00	-4.29
COB (x,y,z) [m]		0.00	0.00	-3.31
Free Surface Center (x,y,z) [m]		-5.12	0.00	0.00
Radius of Gyration at COG [m]	x	12.53	0.00	0.00
	y	0.00	14.33	0.00
	z	0.00	0.00	14.54

TABLE I. Structural properties of the device

The global and body coordinate systems adopted for the hydrodynamic model are identified in Fig. 1. The global coordinate system is identified in blue in Fig. 1 and is at the undisturbed water level directly above the body coordinate system. The incident wave velocity potential φ_o, and hence the phases of the exciting forces, are defined relative to the global coordinate system. The body panels shown in Fig. 2 are defined relative to the center of gravity (COG), which defines the location of the body coordinate system identified in gold in Fig. 1. The body forces and motions calculated by WAMIT are calculated relative to this coordinate system.

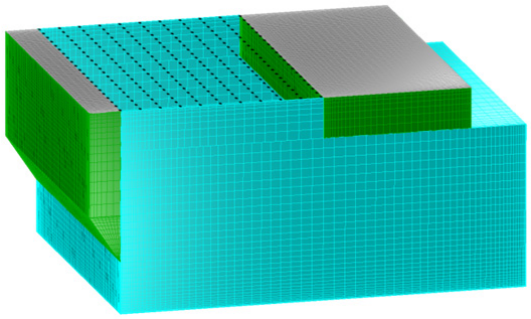

Fig. 2. Wetted surface geometry modeled with cosine spacing in MultiSurf. Dipole panels (cyan), conventional body panels (green), interior surfaces for irregular frequency removal (gray). Black points illustrate the interior field point locations.

Panels representing the 3-dimensional wetted surface of the BBDB are used by the BEM potential flow solver. Fig. 2 illustrates the discretization of panels as well as the types of panels used to solve for the hydrodynamic parameters. The structure panels, green, calculate the wave source potential to obtain the velocity potential. The dipole panels, cyan, obtain the velocity potential without calculation of the source potential. While the grey panels facilitate the removal of irregular frequencies resulting from calculation of the source potential when there is a large waterplane area. Cosine spacing is applied to the panels to increase the accuracy of the calculations close to the corners. The higher-order panel

method is used in WAMIT. Only half of the device is modeled due to the device plane of symmetry at $y = 0$.

An array of 231 field points describing the interior free surface of the BBDB is defined with respect to the global coordinate system. This array is illustrated in Fig. 2 with black points. The field points capture the dynamic pressure and velocity distributions of the free surface.

III. Hydrodynamic Formalism: Reciprocity Relations

Using linear potential flow theory to describe wave structure interactions for a floating OWC, the velocity potential of i moving bodies oscillating in all rigid body modes j with k internal free surfaces is given by:

$$\hat{\phi} = \hat{\phi}_o + \hat{\phi}_d + \sum_{ij} \varphi_{ij} \hat{u}_{ij} + \sum_{k} \varphi_k \hat{p}_k \qquad 1$$

following the notation of [7]. The hat, $\widehat{\ }$, indicates complex amplitudes. The total velocity potential given in Eq. 1 is composed of the incident $\hat{\phi}_o$ and diffracted $\hat{\phi}_d$ potentials as well as the body $\sum_{ij} \varphi_{ij} \hat{u}_{ij}$ and free surface $\sum_k \varphi_k \hat{p}_k$ radiation potentials where $\hat{u}$ is the oscillation velocity and $\hat{p}$ is the pressure. The device treated in this paper contains only one body and one free surface, as shown in Fig. 1, thus $k = i = 1$. From this point forward the velocity potentials, hydrodynamic terms, incident wave amplitude, body velocity, and pressure above the free surface are treated with angular frequency (ω) dependent complex amplitudes and sinusoidal time-dependence $e^{i\omega t}$ with time given by t. Thus hat's, $\widehat{\ }$, will no longer be employed to indicate complex amplitudes.

Given that the state of the floating oscillating water column shown in Fig. 1 must be specified by two parameters, the velocity of the moving body and the pressure in the air chamber, it is clear that there are two coupled hydrodynamic equations relating the total force acting on the body and the total volume flow resulting from air-pressure fluctuations. Each of these equations will be composed of the superposition of the excitation solution found from the incident and diffracted potentials, the radiation solution found from the radiation potentials, and a coupling term uniting them together.

Hence, the total hydrodynamic force, F_{TH}, acting on the j^{th} mode of the body is given by the combination of the excitation force f_j found by holding the body fixed in that direction ($u_j = 0$), the radiated force $\sum_{j'} Z_{jj'} u_{j'}$ found by unit-oscillation velocity $u_{j'}$ of the body without altering the pressure ($p = 0$), and a coupling force H_j^p that accounts for unit-fluctuation of the air-pressure inducing body oscillations:

$$F_{TH,j} = f_j A - \sum_{j'} Z_{jj'} u_{j'} - H_j^p p \qquad j = 1, \dots, 6. \qquad 2$$

In Eq. 2, A is the incident wave amplitude at the global origin and $Z_{jj'}$ is the radiation impedance of the j^{th} mode due to unit-oscillation in one of the six j' rigid body modes.

The total hydrodynamic volume flow, Q_{TH}, resulting from air-pressure fluctuations is given by the excitation volume flow q found by venting the air-chamber to atmosphere ($p = 0$), the radiated volume flow Yp found by unit-fluctuation of the pressure p in the air-chamber without allowing the body to oscillate ($u_j = 0$), and a coupling force H_j^u that accounts for unit-oscillation velocities inducing air-pressure fluctuations:

$$Q_{TH} = qA - Yp - \sum_j H_j^u u_j. \qquad 3$$

In Eq. 3 Y is the radiation admittance of the free surface, and is analogous to the radiation impedance of the oscillating structure.

As will be shown below, each of the hydrodynamic terms identified above can be obtained from a potential flow code without explicitly solving for the radiation potential of the free surface. In this paper WAMIT v6.4 [18] is used to obtain the frequency and directionally dependent hydrodynamic terms.

A. The Floating Body

The hydrodynamic terms relating to a freely oscillating structure are derived using portions of the velocity potential defined in Eq. 1 and they are all standard output of WAMIT v6.4. The excitation force f_j is obtained by:

$$f_j = -i\omega\rho \frac{1}{A} \iint_{S_b} (\phi_o + \phi_d) n_j dS \qquad 4$$

where ρ is the density of seawater, S_b is the wetted surface of the body, and n_j is the unit normal vector pointing into the body. The radiation impedance is found through:

$$Z_{jj'} = i\omega\rho \iint_{S_b} \varphi_j \frac{\partial \varphi_{j'}}{\partial n} dS = b_{jj'} + i\omega a_{jj'} \qquad 5$$

where $b_{jj'} = \mathrm{Re}\{Z_{jj'}\}$ is the radiation resistance and $\omega a_{jj'} = \mathrm{Im}\{Z_{jj'}\}$ is the radiation reactance. An explicit solution of φ_j can be circumvented by solving for the radiation resistance indirectly through a reciprocity relation with the excitation force [7, Eq. 5.148] and solving for the added mass from the radiation resistance through the Kramers-Kronig relationship [7, Eq. 5.105]. The coupling term H_j^p that results from unit-fluctuations of the air-pressure resulting in body movements is found through:

$$H_j^p = i\omega\rho \iint_{S_b} \varphi n_j \, dS \qquad 6$$

where φ is understood to be φ_k with $k = 1$.

Note that the signs of Eq.'s 4, 5, and 6 are switched from the formalism developed in [7] since the unit normal vector must point into the body as a result of the formulation within WAMIT v6.4.

B. The Free Surface

The hydrodynamic terms relating to air-pressure fluctuations above the internal free surface can also be found by using portions of the velocity potential defined in Eq. 1. The excitation volume flow is found through:

$$q = \frac{1}{A} \iint_S \frac{\partial(\phi_o + \phi_d)}{\partial z} dS \qquad 7$$

where the integral is taken over the internal free surface S. This integration is computed discretely by obtaining the excitation vertical velocities, $\frac{\partial(\phi_o+\phi_d)}{\partial z}$, from WAMIT for each field point shown in Fig. 2. The radiation admittance is obtained explicitly through:

$$Y = -\iint_S \frac{\partial \varphi}{\partial z} dS = G + iB \qquad 8$$

where $G = \mathrm{Re}\{Y\}$ and $B = \mathrm{Im}\{Y\}$ are the radiation conductance and radiation susceptance of the internal free surface respectively. Analogous to Eq. 5 above, solution for the radiation admittance does not require the explicit radiation potential φ. As presented in [17], the radiation conductance is related to the excitation volume flow through the following reciprocity relationship:

$$G = \frac{2k}{8\pi\rho g v_g} \int_0^{\pi} |q(\beta)|^2 \, d\beta \qquad 9$$

where the integration from 0 to π already acknowledges the transverse symmetry of the device, β defines the incident wave-headings, and v_g is the group velocity. The radiation susceptance can then be found from the radiation conductance through the Kramers-Kronig relationship:

$$B(\omega) = -\frac{2\omega}{\pi} \int_0^{\infty} \frac{G(y)}{\omega^2 - y^2} dy \qquad 10$$

where the integral is to be understood in the principal value sense and is most readily evaluated with a Hilbert Transformation. The coupling term H_j^u that results from unit-oscillation velocities resulting in air-pressure fluctuations is found through:

$$H_j^u = -\iint_S \frac{\partial \varphi_j}{\partial z} dS = C_j + iJ_j \qquad 11$$

where the integral is taken over the internal free surface S. This integration is computed discretely by obtaining the radiation vertical velocities $\frac{\partial \varphi_j}{\partial z}$ from WAMIT for each field point shown in Fig. 2. WAMIT User Manual v6.4 in Section 4.7 [18] does not state the correct non-dimensional form of the radiation velocities. The correct non-dimensional form of the radiation velocity for the j^{th} mode is presented in User Manual v7.0 [16] and given below:

$$\bar{u}_j = \frac{\omega^2 L}{g} \bar{\nabla} \bar{\varphi}_j = \frac{\omega^2 L U}{g L^n u_j}. \qquad 12$$

Here L is a scaling factor representative of the length of the device, $\bar{\nabla}$ is the non-dimensional gradient operator, n is dictated by the rigid mode j ($n = 0$ for $j = 1,2,3$ and $n = 1$ for $j = 4,5,6$), U is the dimensional fluid velocity, and u_j is the dimensional velocity of the body in the j^{th} mode.

Finally it can be shown that $H_j^p = -H_j^u$ and hence explicitly solving for the radiation potential φ of the free surface is unnecessary to determine all of the hydrodynamic parameters.

A transformation vector is required to account for the velocity of the body at the center of the free surface in the global coordinate system due to body motions around the COG (as defined in the body coordinate system). Thus the vertical velocity of the body at the center of the internal free surface is calculated through multiplication of the body velocity with the transformation vector:

$$\boldsymbol{T} = [0 \quad 0 \quad 1 \quad 0 \quad -r' \quad 0]^{\mathrm{T}} \qquad 13$$

where r' is identified in Fig. 1 and TABLE I. This transformation relativizes the air-chamber results to the movements of the structure.

IV. Hydrodynamic Results

The hydrodynamic parameters are found for wave frequencies spanning 0 to 2.5 rad/s in 0.01 rad/s intervals assuming infinite depth. The integral in Eq. 9 requires a sum over incident wave propagations. Therefore hydrodynamic parameters are found for 17 distinct wave-headings starting with incidence in the positive x-direction ($\beta = 0$) and increasing in intervals of $\pi/16$. However, the only wave-heading analyzed to estimate performance is $\beta = 0$.

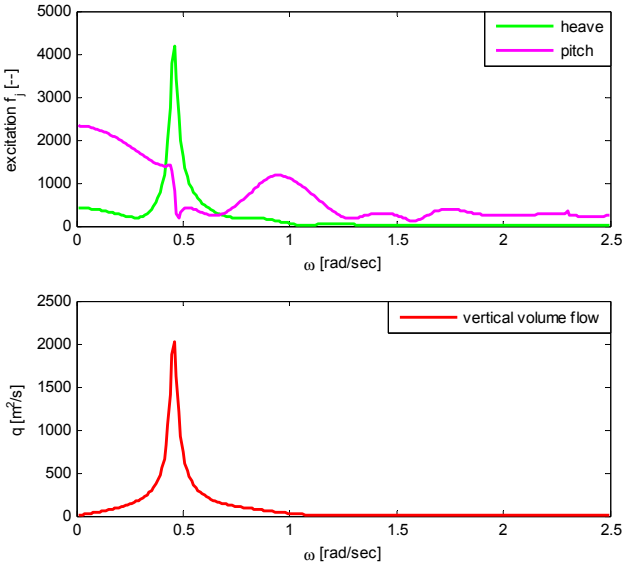

Fig. 3: Non-dimensional excitation forces on the structure in heave and pitch as well as the excitation volume flow of the free surface.

Fig. 3 shows the initial excitations from the incident and diffracted velocity potentials for both the oscillating structure f_j in heave and pitch as well as the excitation volume flow q. The secondary peak in pitch excitation begins after $\omega = 0.7$ and obtains it's maximum value at $\omega \cong 0.95$.

The radiation impedance for the structure and the radiation admittance for the oscillating water column are shown in Fig. 4, Fig. 5, and Fig. 6. Fig. 4 and Fig. 5 show the non-dimensional heave and pitch damping terms and added mass/inertia respectively. Unlike axisymmetric devices, non-axisymmetric devices exhibit a cross-coupling between the heave-pitch and the heave-surge rigid body modes, hence the radiation impedance cross-coupling terms are non-zero and appreciable for this device. These cross-couplings influence the locations of the natural resonances of the freely floating structure [27]. Furthermore, the hydrodynamic coupling

between the structure and air column is derived from the radiation potential, φ_j, thus we expect from Eq.'s 3 and 11 that both surge and pitch will contribute to the air-pressure fluctuation through the coupling term H_j^u.

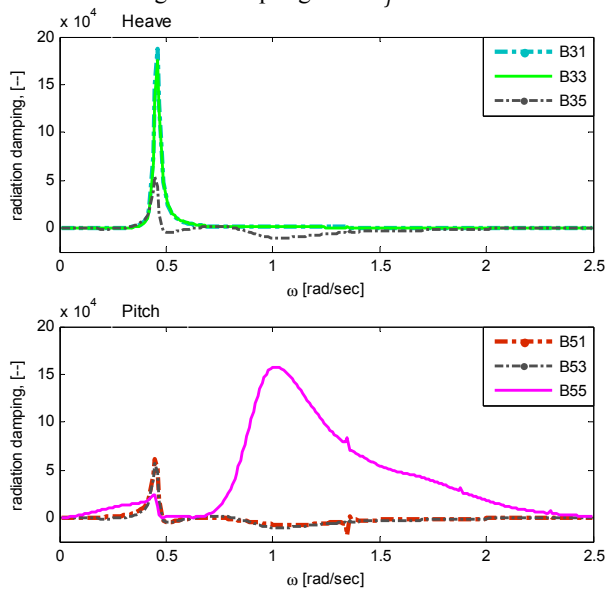

Fig. 4: Non-dimensional radiation damping as a function of frequency for heave and pitch.

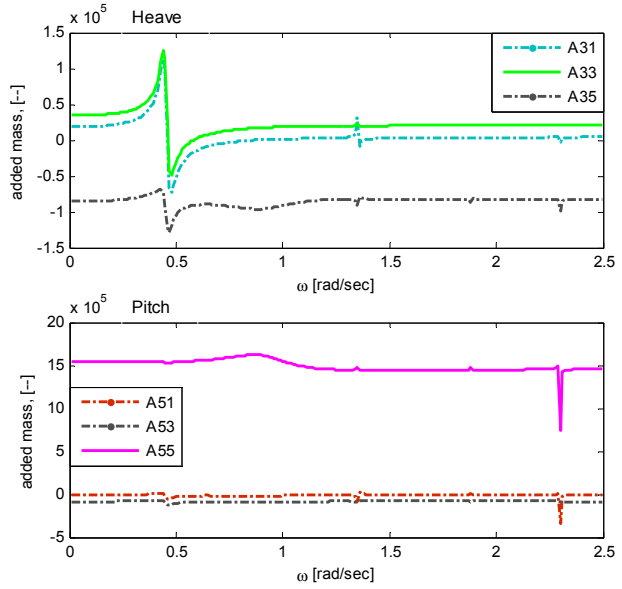

Fig. 5: Non-dimensional added mass/inertia as a function of frequency for heave and pitch.

For a fixed structure OWC, the resonance of the OWC is solely defined by the excitation q and radiation admittance Y. Hence, for an uncoupled system the radiation susceptance, shown with the conductance in Fig. 6, identifies the resonance since it includes the effect of the hydrostatic stiffness [7]. Thus the first zero-crossing is identified as the piston resonance location of the hydrodynamically uncoupled system. The large peaks occurring in Fig. 3-Fig. 7 are localized in frequency with the first zero-crossing of the radiation susceptance.

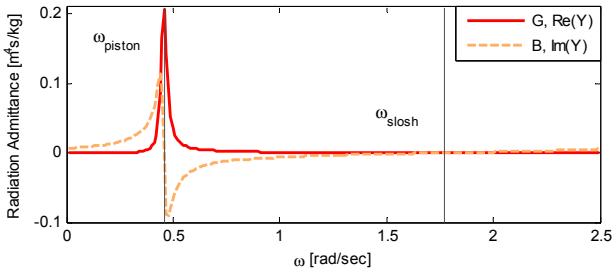

Fig. 6: Radiation conductance and susceptance of the fluctuating air-pressure. The hydrodynamically uncoupled piston and slosh resonances are identified

Fig. 7 shows the real and imaginary components of the heave and pitch coupling terms H_j^u. As expected the magnitude of coupling is quite large in each mode indicating that an oscillating structure will induce a measurable air-pressure fluctuation, or equivalently an air-pressure fluctuation will induce structure motions.

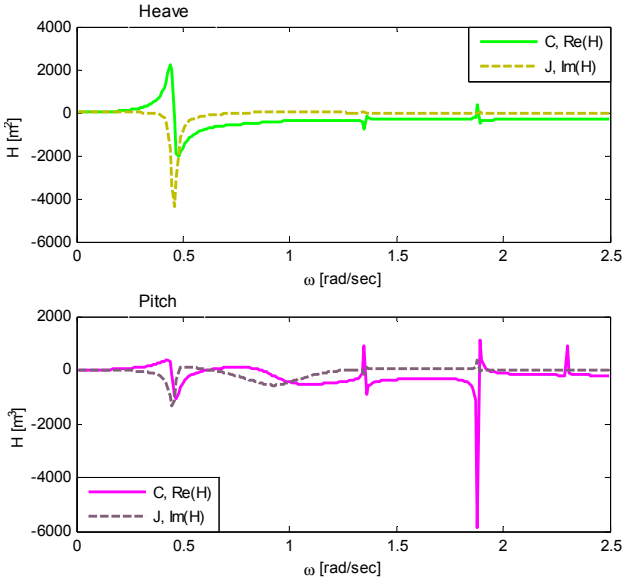

Fig. 7: Coupling terms for heave and pitch motions of the body showing strongly coupling to the fluctuating air-pressure.

As shown in Eq. 3 this coupling influences the solution for the pressure response. The hydrodynamically coupled relative pressure response amplitude operator (RAO) can be derived from Eq. 3 and 13 to be:

$$\frac{p}{A} = \frac{q - \sum_j (H_j^u + T_j S) u_j}{Y}. \qquad 14$$

where the coupling term H_j^u is modified by the transformation vector $\boldsymbol{TS}$ to account for the pressure-volume flow that occurs due to the velocity of the body at the center of the free surface. The non-zero contribution of H_3^u and H_5^u, as well as H_1^u, seen in Fig. 7 signify that the natural resonance of the OWC has the potential to be highly influenced by these coupling terms. Hence, the resulting fluctuating air-pressure resonance could

migrate due to the coupling with surge, heave, and pitch structural modes in much the same way that the heave structural resonance migrates due to the influence of the rigid-body cross-coupling terms. Fig. 8 shows the magnitude and phase of the numerator of the hydrodynamically coupled relative pressure RAO detailed in Eq. 14.

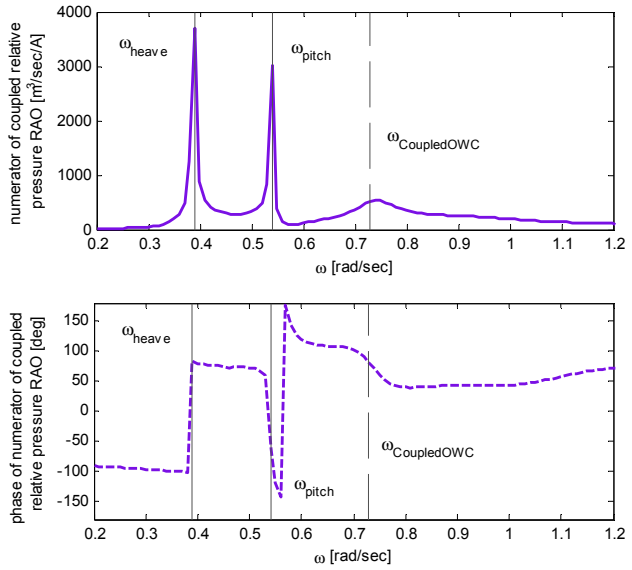

Fig. 8: Numerator of hydrodynamically coupled, but unlinked, pressure RAO. Magnitude of peak and phase change at $\omega = 0.73$ indicate's the OWC resonance location for the hydrodynamically coupled system.

Three peaks are identified in Fig. 8: two are structural in origin (solid lines) and one is from the hydrodynamic coupling with the oscillating water column (dashed line). The two structural resonances correspond to heave ($\omega = 0.39$) and pitch ($\omega = 0.55$) and are close to estimates obtained using standard equations [27] which do not produce accurate estimates for non-axisymmetric devices. The uncoupled piston resonance identified in Fig. 6 is not visible in Fig. 8 and the phase of the numerator is constant at this frequency. The third peak seen in Fig. 8 at $\omega = 0.73$ could originate from two places: 1) this peak is a result of the structure motions solely (similar to the explanation of the first two peaks) or 2) it is the new resonance location for the coupled OWC.

If option one is correct, then the system is so misbalanced that dynamics of the structure are completely overwhelming the dynamics of the water column and we thus do not see the piston resonance identified in Fig. 6. Since there is a large pitch excitation near this third peak (as indicated above in Fig. 3) it is possible that this excitation results in a large pitch rotational velocity and is the base cause of this last peak.

However, the authors believe that the last peak in Fig. 8 is the coupled OWC resonance and this is further supported in Section VI. This new resonance location for the oscillating water column is a direct result of the dynamics of the oscillating structure. A steady change in phase is associated with this peak and this type of resonance is often associated with damped systems. In this case, the non-zero B seen in Fig. 6 would offer this damping.

V. Linked Governing Equations for Floating OWC

A linear frequency-domain model is used to produce estimates of the power conversion capabilities of the device presented in Fig. 1. There are two governing equations: one for the oscillating structure and one for the fluctuating air-pressure. The power conversion chain links the oscillating structure to the OWC through the resistive damping term R_{load}. The governing equation for each mode of the oscillating structure is given by:

$$\begin{aligned} & i\omega m_{jj'} u_j \\ &= \left(f_j A - \left(b_{jj'} + i\omega a_{jj'}\right) u_j \right. \\ &\left. - \left(-H_j^u + T_j S\right)p\right) - \left(\frac{1}{i\omega} C_{jj'} u_j\right) - \left(\frac{1}{i\omega} K_j u_j\right) \\ &- \left(b_{vis,j} u_j\right) \end{aligned} \qquad (15)$$

where the left-hand side of the equation is the total force acting on the body. The first term on the right-hand side is the hydrodynamic contribution discussed in previous sections. The second term, technically part of the full hydrodynamic contribution, is the hydrostatic restoring force. The third and fourth terms are added to account for additional forces affecting the device: the mooring restoring force and the linearized viscous damping both represented here as diagonal matrices.

A Wells Turbine, which possesses a linear relationship between pressure and flow, is assumed in this performance model. Since air is highly compressible, accurate predictions of the air flow through the Wells Turbine require a linear representation of this compressibility. The governing equation for the relative air flow through the Wells Turbine is given by:

$$\begin{aligned} & \left(\frac{1}{R_{load}} + i\frac{\omega \forall_o}{\gamma p_{atm}}\right) p \\ &= \left(qA - (G + iB)p - \sum_j \left(H_j^u + T_j S\right) u_j\right) \\ &- \frac{1}{R_{vis}} p \end{aligned} \qquad (16)$$

where the left-hand side of the equation is the total compressible relative air flow through the Wells Turbine (consistent with [28]) with no limitation on the pressure allowed within the air-chamber. The linearized air compressibility is defined through the following terms: the initial volume is $\forall_o$, $\gamma = 1.4$ and is the ratio between the constant-pressure and constant-volume specific heats for air, and p_{atm} is the atmospheric pressure. The first term on the right-hand side is the hydrodynamic contribution discussed in previous sections. The second term is added to account for the viscous damping in a linearized manner. Note that smaller R_{vis} results in greater losses of the volume flow. This inverse representation has been selected based on the formalism developed in [7] where analog's to electric circuitry are heavily employed and admittance is the inverse of impedance.

These coupled governing equations are most readily understood in matrix notation as follows:

$$\begin{pmatrix} \boldsymbol{f} \\ q \end{pmatrix} A = \begin{pmatrix} \boldsymbol{Z}_i & -\boldsymbol{H}_i \\ \boldsymbol{H}_i^T & Y_i + \dfrac{1}{R_{load}} \end{pmatrix} \begin{pmatrix} \boldsymbol{u} \\ p \end{pmatrix} \quad 17$$

where the bolded quantities are matrices or column vectors and:

$$\boldsymbol{Z}_i = \boldsymbol{b} + \boldsymbol{b}_{vis} + i\omega \left(\boldsymbol{m} + \boldsymbol{a} - \frac{(\boldsymbol{C} + \boldsymbol{K})}{\omega^2} \right), \quad 18$$

$$\boldsymbol{H}_i = \boldsymbol{H} + \boldsymbol{T}S, \text{ and} \quad 19$$

$$Y_i = \left(G + \frac{1}{R_{vis}} \right) + i \left(B + \frac{\omega \forall_o}{\gamma p_{atm}} \right). \quad 20$$

The linked governing equations above can then be solved to obtain the linked body velocity RAO and the linked relative pressure RAO. The RAO's are the response of a variable at a given frequency per unit incident wave amplitude A. The relative volume flow through the Wells Turbine may be derived from:

$$Q_T = qA - Y_i p - \boldsymbol{H}_i^T \boldsymbol{u} = \frac{p}{R_{load}}. \quad 21$$

From the relative volume flow, the relative interior free surface elevation may then be derived from:

$$\frac{\xi_{\text{Rel,FSE}}}{A} = -\frac{Q_T / A}{i\omega S}. \quad 22$$

The negative sign in Eq. 22 reflects the fact that positive volume flow into the air-chamber occurs for a decreasing free surface elevation.

The power absorbed by the coupled and linked device is dependent upon the R_{load} applied at the air turbine. The pneumatic power available to the Wells Turbine from the air-column is the product of the relative pressure in the air-chamber and the relative volume flow [7]

$$\langle P \rangle = \overline{p(t) Q_T(t)} = \frac{1}{2} Re\{p Q_T^*\}. \quad 23$$

The pressure, p, is found through solution of Eq. 17 and is the relative pressure resulting from both the movements of the structure as well as the water column. In monochromatic waves, the average pneumatic power simplifies to

$$\langle \mathrm{P} \rangle = \frac{1}{2} \frac{1}{R_{load}} |p|^2. \quad 24$$

The magnitude of the resistive damping term will impact the pneumatic power available to the Wells Turbine by influencing both the motion of the device as well as the water column.

A. Optimal Resistive Damping

The optimal resistive damping term can then be found from the solution to the following optimization condition

$$\frac{\partial \langle \mathrm{P} \rangle}{\partial R_{load}} = 0. \quad 25$$

where $\langle P \rangle$ is the average power presented in Eq. 24. Application of the optimization condition presented in Eq. 25 results in the following analytic form of the frequency dependent optimal resistive damping:

$$R_{l_{opt}} = (|Y_i + \boldsymbol{H}_i^T \boldsymbol{Z}_i^{-1} \boldsymbol{H}_i|^2)^{-\frac{1}{2}}. \quad 26$$

Eq. 26 is the optimal resistive damping for a floating OWC. If the structure were fixed, the optimal R_{load} would consist of only the first term in Eq. 26. However, since the structure is floating, and also absorbing power from the incident waves, the optimal resistive damping must reflect the contribution from the floating structure. Hence the additional term relating to the magnitude of coupling $\boldsymbol{H}_i$ and the radiation impedance $\boldsymbol{Z}_i$ of the structure in the analytic form of the optimal R_{load} is reasonable. Inserting Eq. 26 into Eq. 24 produces the maximum pneumatic power in monochromatic waves.

VI. Performance Results: Monochromatic Waves

Viscous damping terms were selected in order to reduce the magnitudes of the linked body motions and free surfaces elevations at resonance. Constant (and diagonal when applicable) damping values for both the body and the free surface are applied across all frequencies. For the presented solutions these are: $b_{vis} = 0.02\sqrt{M_{tot} c_{tot}}$ and $R_{vis}^{-1} = 0.01(\max(G))$. M_{tot} is the physical mass in combination with the infinite frequency added mass and c_{tot} is the total restoring force (hydrostatic plus mooring). The magnitude of these additional viscous damping terms should be verified with experimental tests. However the presented values are able to reduce RAO magnitudes to reasonable levels.

The mooring restoring force is obtained from the mooring design detailed in [29]. The design was found to act linearly for excursions of $\pm$ 5m in the surge, sway, and heave directions. The magnitudes of the restoring forces are: 55.5 kN in surge, 6.1 kN in sway, and 7.5 kN in heave.

A. Optimal Resistive Damping

Fig. 9 compares the analytic expression of $R_{l_{opt}}$ from Eq. 26 as a function of frequency to a numeric optimization. The difference between the curves is solely a result of the fidelity of the numeric optimization, which confirms the solution presented in Eq. 26. Since both the body motions and the free surface are accounted for in the relative pressure term, the profile of $R_{l_{opt}}$ experiences multiple distinct minima corresponding to natural resonances for the coupled device. The structural resonance locations and the coupled OWC resonance location are identified in Fig. 9 for clarity (solid and dashed vertical lines, respectively). Between these minima, $R_{l_{opt}}$ increases resulting in three resistive damping peaks.

Fig. 10 compares the linked and unlinked RAO's for heave, pitch, and the absolute free surface elevation (FSE) when $R_{l_{opt}}$ is applied at each frequency. The linked RAO's exhibit the unlinked natural resonances as would be expected since $R_{l_{opt}}$ is minimal at these locations. However, the linked RAO's also exhibit additional peaks that correspond to the peaks seen in $R_{l_{opt}}$. These new linked peaks are the result of

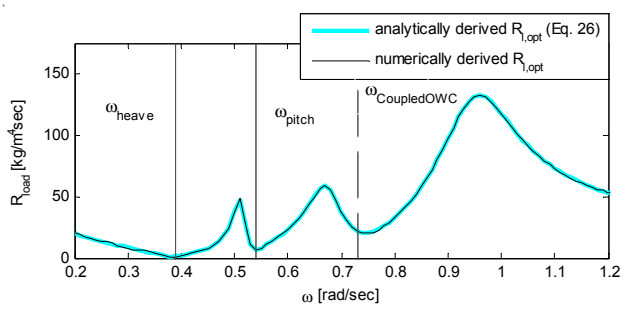

Fig. 9: Comparison of analytically derived and numerically obtained optimal resistive damping $\boldsymbol{R_{l_{opt}}}$ for a floating OWC.

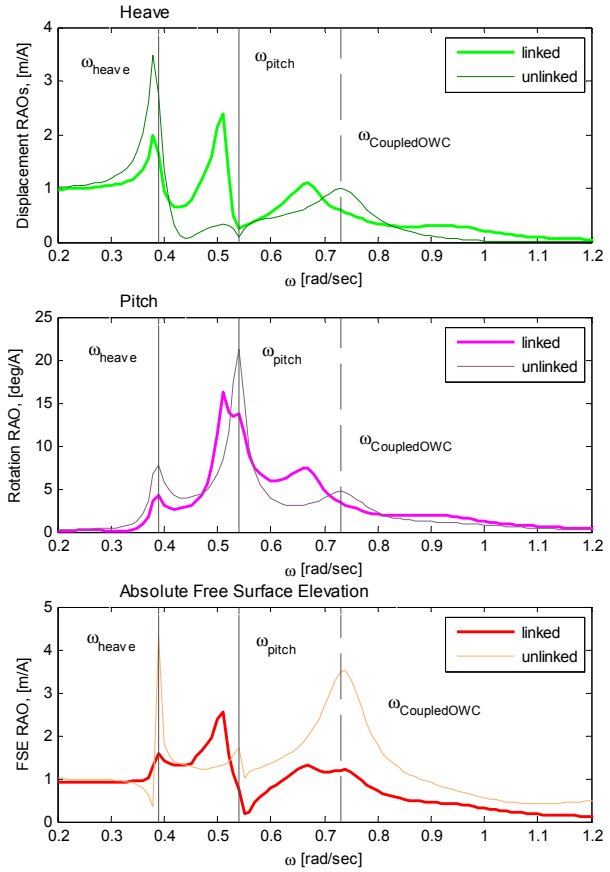

Fig. 10: RAO's for heave, pitch, and the absolute free surface elevation when a Wells Turbine with $\boldsymbol{R_{l_{opt}}}$ is applied in the linked case and when there is no Wells Turbine in the unlinked case.

the free surface and structure moving nearly in phase with one another.

Fig. 11 focuses on the phase relationship for the RAO's presented in Fig. 10. The locations of the peaks in $R_{l_{opt}}$ are identified with vertical dotted lines; these coincide with the phase of the FSE matching the phase of the structural RAOs. Comparing the phase of linked heave with linked absolute free surface elevation at $\omega = 0.51$ shows that the two are nearly in phase. Similar inspection at $\omega = 0.67$ between the pitch and absolute free surface elevation also shows a close phase match. Additionally, at $\omega = 0.67$ the phase of the heave RAO is similar to the pitch and FSE. Hence it is not clear that this peak is purely a pitch-coupled OWC peak as identified. The last peak in Fig. 9 located at $\omega = 0.96$ is identified in all three figures and it is clear that there again appears to be a close phase match.

Work by Alves [30] has shown the effect of accounting for both the oscillating structure and the fluctuating air-pressure with a one-dimensional, axisymmetric, floating OWC device modeled using generalized modes. His results also show a new peak between the structural heave resonance and the coupled OWC resonance. This third peak is the linked heave-coupled OWC peak that is the result of both the body and the

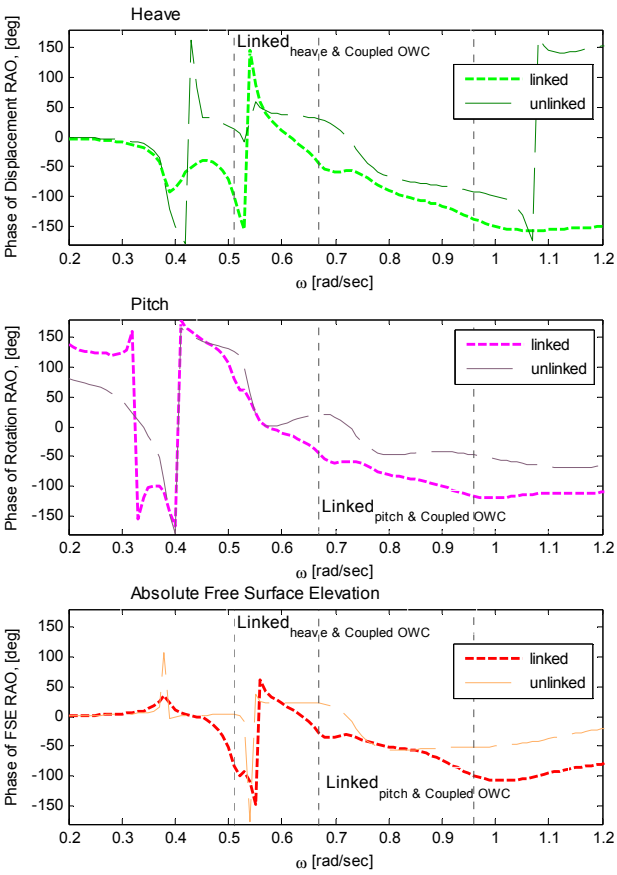

Fig. 11: Phases of the RAO's for heave, pitch, and the absolute free surface elevation when a Wells Turbine with $\boldsymbol{R_{l_{opt}}}$ is applied in the linked case and when there is no Wells Turbine in the unlinked case.

fluctuating air-pressure oscillating in phase but with distinct amplitudes. The three new peaks in Fig. 10 can be similarly explained through their corresponding phase relationships in Fig. 11. Hence, the linked heave-coupled OWC, the linked pitch-coupled OWC, and the last peak exhibit the same pattern expected from Alves' one-dimensional results.

This interpretation of the linked peaks also lends itself to the belief that the resonance peak at $\omega = 0.73$ is the coupled OWC peak. Additionally, the largest unlinked RAO response from the absolute FSE in Fig. 10 is at this frequency.

The relative linked pressure is shown in Fig. 12. The peaks in pressure correspond to the locations of increased resistive damping. Alternatively the peaks in relative volume flow, shown in Fig. 13, correspond to resonances in the system. This inverse partnership between pressure and flow is expected: when the device is in resonance there will be large volume flow, otherwise $R_{l_{oad}}$ will be used to increase the pressure in the air-chamber when the phase relationships have a close phase match.

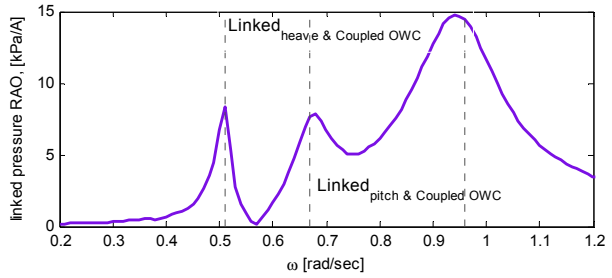

Fig. 12: RAO of relative linked pressure with $\boldsymbol{R_{l_{opt}}}$ applied.

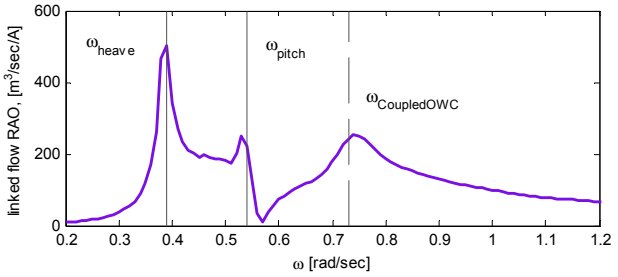

Fig. 13: RAO of relative linked flow with $\boldsymbol{R_{l_{opt}}}$ applied.

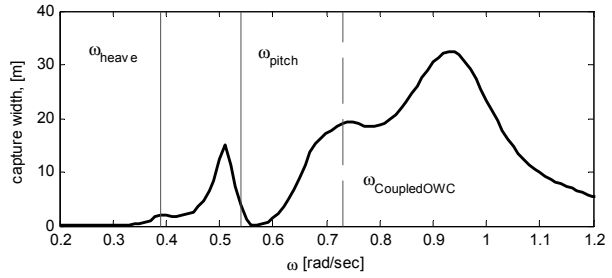

Fig. 14: Capture width for a floating OWC with $\boldsymbol{R_{l_{opt}}}$ applied at each frequency.

Finally the capture width of this device, with $R_{l_{opt}}$ applied at each frequency, is shown in Fig. 14; the locations of the resonances are identified. Both the heave and the coupled OWC resonance contribute to the capture width. The pitch natural resonance is not detectable, but it is likely that it has been subsumed into the linked heave-coupled OWC peak. The three peaks in Fig. 9 that result from the phase matching between degrees of freedom strongly effects the structure of the capture width. Linking the structure to the OWC through the Wells Turbine and applying $R_{l_{opt}}$ results in the largest power conversion at these linked peaks.

Although coupling between the structure and the OWC is often mentioned as a benefit of the BBDB design, this is the first presentation, to the authors' knowledge, demonstrating the linked heave-coupled OWC and linked pitch-coupled OWC modes. These linked modes expand the area of power conversion and cannot be ignored.

VII. Conclusions

Results presented here provide a resistive control strategy to optimize converted power for a floating OWC device. Further, the dynamics of a floating OWC are shown to be distinct from those of a fixed device. The relative motion of the water column for a non-axisymmetric device results in multiple resonance peaks and a broadening of the capture width of the device. Additionally, the resonance location of a floating OWC has been shown to be distinct from the fixed OWC resonance location.

A linear, frequency-domain, performance model is presented that links the oscillating structure to air-pressure fluctuations with a Wells Turbine. The hydrodynamic parameters related to the fluctuating air-pressure within the OWC are calculated using reciprocity relations on an array of field points defining the interior free surface. Device structural parameters for a non-optimized BBDB are detailed. Dimensions of the device were informed from literature while the structural properties were obtained from an idealized solid model. The performance model is exercised on this device using the calculated hydrodynamic parameters. The air is modeled as a compressible system. Viscous damping values are applied to both the structure and the air column.

The resonances of an OWC contained in a floating body are not solely defined by the excitation q and radiation admittance Y as it is for a fixed structure. For a fixed OWC, resonance is determined by the first B zero-crossing. However, for a floating OWC, coupling between the oscillating structure and the fluctuating air-pressure indicates that the resonance of the OWC moves to a new location.

An analytic expression to determine the optimal $R_{l_{oad}}$ for any floating OWC is presented. This expression is modified from the fixed OWC expression by a term relating to the magnitude of coupling $\boldsymbol{H}_i$ and the radiation impedance $\boldsymbol{Z}_i$ of the structure.

Performance model results are presented for the optimal $R_{l_{oad}}$. Results include RAO's of the device motion and internal free surface height as well as the relative pressure and volume flow in the air-chamber. Additionally the optimal capture width is presented. The results exhibit that it is possible to preserve the unlinked natural resonances and that the linked modes, resulting from the peaks in $R_{l_{opt}}$, substantially increase the capture width of the BBDB.

Acknowledgment

The authors would like to acknowledge helpful conversations with Adi Kurniawan, Paul Palo, Marco Alves, and staff at HMRC. The authors would like to acknowledge clarifications from WAMIT's Nick Newman and Chang-Ho Lee. The authors would like to acknowledge the help of Guild

Copeland in the creation of solid models. Additionally the authors would like to acknowledge the thoughtful questions from the reviewers; derivation of Eq. 26 and the final form of this paper are a result of their questions.

This work was funded by the Department of Energies' Wind and Water Power Technologies Office. Sandia National Laboratories is a multi-program laboratory managed and operated by Sandia Corporation, a wholly owned subsidiary of Lockheed Martin Corporation, for the U.S. Department of Energy's National Nuclear Security Administration under contract DE-AC04-94AL85000.

REFERENCES

[1] Ocean Energy Ltd., "Ocean Energy OEBuoy: A Backward Bent Duct Design." [Online]. Available: http://www.oceanenergy.ie/.

[2] Oceanlinx Ltd., "Oceanlins'x blueWAVE (offshore) and greenWAVE (nearshore)." [Online]. Available: http://www.oceanlinx.com/.

[3] Embley Energy Ltd., "Embley Energy's Sperboy." [Online]. Available: http://www.sperboy.com/index.html?_ret_=return.

[4] A. F. de O. Falcao, "The shoreline OWC wave power plant at the Azores," presented at the 4th European Wave Energy Conference, Aalborg, Denmark, 2000.

[5] Heath, T, Whittaker, TJT, and Boake, CB, "The design, construction and operation of the LIMPET wave energy converter (Islay, Scotland)," presented at the 4th European Wave Energy Conference, Aalborg, Denmark, 2000.

[6] Y. Torre-Enciso, I. Ortubia, L. I. López de Aguileta, and J. Marqués, "Mutriku wave power plant: from the thinking out to the reality," in *Proceedings 8th European Wave Tidal Energy Conference*, 2009, pp. 319–29.

[7] Johannes Falnes, *Ocean Waves and Oscillating Systems*. New York: Cambridge University Press, 2002.

[8] Y. Masuda, T. Yamazaki, Y. Outa, and M. McCormick, "Study of backward bent duct buoy," in *OCEANS'87*, 1987, pp. 384–389.

[9] Fukuda, K., "Behaviour of water in vertical well with bottom opening of ship, and its effect on ship motions," *Journal of Naval Architects of Japan*, vol. 141, pp. 107–122, 1977.

[10] Y. Wei, J. Yang, G. Chen, and Z. Hu, "The Research of Moonpool Size Effect on the Hydrodynamic Performance of FDPSO," in *Proceedings of the ASME 2011 30th International Conference on Ocean, Offshore and Arctic Engineering*, Rotterdam, The Netherlands, 2011, pp. 459–467.

[11] D. V. Evans, "The Oscillating Water Column Wave-energy Device," *IMA J Appl Math*, vol. 22, no. 4, pp. 423–433, Dec. 1978.

[12] D. V. Evans, "Wave-Power Absorption by Systems of Oscillating Surface Pressure Distributions," *Journal of Fluid Mechanics*, vol. 114, pp. 481–499, 1982.

[13] A. J. N. A. Sarmento and A. F. de O. Falcão, "Wave generation by an oscillating surface-pressure and its application in wave-energy extraction," *Journal of Fluid Mechanics*, vol. 150, pp. 467–485, 1985.

[14] Lee, C.-H., Newman J.N., and Nielsen F.G., "Wave interactions with an oscillating water column," in *Proceedings International Offshores and Polar Engineering Conference*, Los Angeles, 1996.

[15] C. H. Lee and F. G. Nielson, "Analysis of oscillating-water column device using a panel method," presented at the 11th International Workshop on Water Waves and Floating Bodies, Hamburg Germany, 1996.

[16] *WAMIT v7.0*. Chestnut Hill, Massachusetts: WAMIT, Inc.

[17] Kurniawan, A, Hals, J, and Moan, Torgeir, "Modeling And Simulation Of A Floating Oscillating Water Column," in *Proceedings of the ASME 2011 30th International Conference on Ocean, Offshore and Arctic Engineering*, Rotterdam, The Netherlands, 2011.

[18] *WAMIT v6.4*. Chestnut Hill, Massachusetts: WAMIT, Inc.

[19] *3D CAD Design Software SolidWorks*. Dassault Systèmes SolidWorks Corp.

[20] *MultiSurf*. Southwest Harbor, Maine: AeroHydro, Inc.

[21] Y. Imai, K. Toyota, S. Nagata, T. Setoguchi, and M. Takao, "An Experimental Study on Generating Efficiency of a Wave Energy Converter" Backward Bent Duct Buoy," presented at the EWTEC.

[22] M. Suzuki, T. Kuboki, S. Nagata, and T. Setoguchi, "Numerical Investigation of 2D Optimal Profile of Backward-Bent Duct Type Wave Energy Converter," *J. Offshore Mech. Arct. Eng.*, vol. 133, no. 4, pp. 041602–8, Nov. 2011.

[23] D. Hong, S. Hong, and S. Hong, "Numerical study on the reverse drift force of floating BBDB wave energy absorbers," *Ocean engineering*, vol. 31, no. 10, pp. 1257–1294, 2004.

[24] Copeland, Guild and Bull, Diana, "BBDB Structural Model: Simplified Modular Design." Internal Report. Not Yet Published.

[25] Epler, Jeff, "OWC Device Components, Dimensions, Design Standards, Mass & Inertia Estimates," ReVision Consulting, 25-Jan-2012. Internal Report. Not Yet Published.

[26] Previsic, Mirko, "OWC Power Conversion Chain Weight Estimate," 10-Jan-2012. Personal Communication.

[27] J. N. Newman, *Marine hydrodynamics*. MIT Press, 1977.

[28] A. Brendmo, J. Falnes, and P. Lillebekken, "Linear modelling of oscillating water columns including viscous loss," *Applied ocean research*, vol. 18, no. 2, pp. 65–75, 1996.

[29] D. Bull and P. Jacob, "Methodology for creating nonaxisymmetric WECs to screen mooring designs using a Morison Equation approach," in *OCEANS '12. "Harnessing the Power of the Ocean". Proceedings*, Hampton Roads, VA, 2012, pp. 1 –9.

[30] M. A. de A. Alves, "Numerical Simulation of the Dynamics of Point Absorber Wave Energy Converters using Frequency and Time Domain Approaches," UNIVERSIDADE TÉCNICA DE LISBOA, INSTITUTO SUPERIOR TÉCNICO, 2011.